동력시스템공학회지 제28권 제3호 pp. 21-32 2024년 6월 ISSN 2713-8429(Print) ISSN 2713-8437(Online)
Journal of Power System Engineering https://doi.org/10.9726/kspse.2024.28.3.021
Vol. 28, No. 3, pp. 21-32, June 2024

Design of Robust Decoupling Controller for 6-DoF Active Vibration Isolation System

Tan-Ngoc Nguyen*, Thinh Huynh**, Dong-Hun Lee** and Young-Bok Kim*†

(Received 28 March 2024, Revision received 08 May 2024, Accepted 10 May 2024)

Abstract : Active vibration isolation system (AVIS) is one of the latest applications for improving the working performance of high-precision devices, which are easily affected by environmental vibrations. Additionally, a major challenge with such a high degree-of-freedom (DoF) system is the interaction among individual movements. Therefore, this paper introduces the design of a robust decoupling controller for the 6-DoF AVIS. The mathematical model of the system is presented; the decoupling process is outlined; and the mixed sensitivity H_∞ control framework is used to develop the robust decoupling controller. The effectiveness of the proposed system is demonstrated by comparing simulation results of its velocities and control efforts with the results of an uncontrolled system, a PID control system, and a robust control system. The designed controller ensures robustness and decoupling performance through the suppression of external vibrations, isolation of interactions, and stabilization of the system.

Key Words : Active Vibration Isolation System (AVIS), Degree of Freedom (DoF), Mathematical Modeling, Robust Decoupling Control

1. Introduction

In the field of mechanical engineering, vibration is inevitable, regarding of both free vibration inherent in systems and forced vibration originating from the mechanical system's operation and its surroundings. These vibrations carry numerous negative consequences, including machine malfunctions, excessive power consumption, and equipment damage.[1-3] Their impact is particularly critical in high-precision fields such as microscopy, aircraft engineering, and gravitational wave detections. The increased performance standards for precision instruments establish strict limitations on mechanical vibrations. Consequently, without effective vibration isolation, the objectives of electron microscopy and high-precision devices, in general, remain unattainable. A standard vibration isolation system comprises two main components: the need-to-isolate platform, also known as the top platform, and the supporting platform, referred to as the base platform. The vibration isolation mechanisms are placed between the two platforms.

The most basic method for vibration isolation is to use a passive system (PVIS). This system typically consists of mechanical elements like

* † Young-Bok Kim(https://orcid.org/0000-0001-6035-6744) : Professor, Department of Intelligent Robot Engineering, Pukyong National University.
E-mail : kpjiwoo@pknu.ac.kr, Tel : 051-629-6197
*Tan-Ngoc Nguyen(https://orcid.org/0000-0002-0097-6391) : Graduate student, Department of Intelligent Robot Engineering, Pukyong National University.
**Thinh Huynh(https://orcid.org/0000-0001-7329-8432), Dong-Hun Lee(https://orcid.org/0000-0001-6157-9763) : Assistant Professor, Department of Smart Mobility Engineering, College of Information Technology and Convergence, Pukyong National University.

springs and dampers positioned between the two platforms, creating a connection. The springs work in conjunction with the dampers to eliminate vibrations from the ground and suppress amplified oscillations within the system. This, in turn, stabilizes the top platform, ensuring the performance for high-precision devices. Despite its advantages, including no energy consumption, a simple structure, low cost, and effective suppression of high-frequency vibrations, PVIS has limitations. Vibration isolation is not actively controlled, as the system is driven by the vibrations themselves. Consequently, achieving consistent isolation performance, especially in low-frequency zone, becomes challenging, and the system is vulnerable to disturbances. Another significant drawback is that, in the resonant frequency zone, the system's vibrations are amplified due to the characteristics of its structure.[3-5)]

Active vibration isolation systems are designed to overcome the limitations of the PVISs by ensuring effective vibration suppression across a wide frequency range. The AVIS structure is similar to the PVIS, but with the different in installing actuators and sensors between the two platforms. Hence, vibration suppression is achieved through the utilization of sensors to collect the motion and actuators to regulate it. Essentially, a well-designed control algorithm is implemented to accomplish the goal of vibration isolation. Nevertheless, in order to attain the vibration stabilization of the 6-DoF AVIS, the amount of actuators must be greater or, at least, equal to the number of controlled degrees of freedom. This gives rise to the challenge that the AVIS typically becomes an over-actuated system.[6-8)] Unfortunately, the addition of surplus actuators worsens the problem of interactions in the AVIS. Nonetheless, the design of the control system necessitates not only the decoupling of interactions but also the fulfillment of the system's performance requirements.

In this research, a novel robust decoupling control system for the 6-DoF AVIS is introduced. The primary objective is to isolate ground vibrations affecting the top platform, which supports high-precision devices, and another objective is to eliminate interactions among each degree of freedom in the 6-DoF AVIS. To achieve these objectives, a feedforward compensator is designed to suppress the impact of interactions in each input-output pair of the 6-DoF AVIS. Subsequently, a feedback controller is developed based on the mixed sensitivity H_∞ framework. The effectiveness of the proposed control system is verified through simulation results.

2. System Modeling

2.1 System Description

The diagram illustrating the proposed 6-DoF AVIS is presented in Fig. 1. The top platform, where high-precision devices operate, requires isolation from ground vibrations to maintain optimal device performance. The connection between the

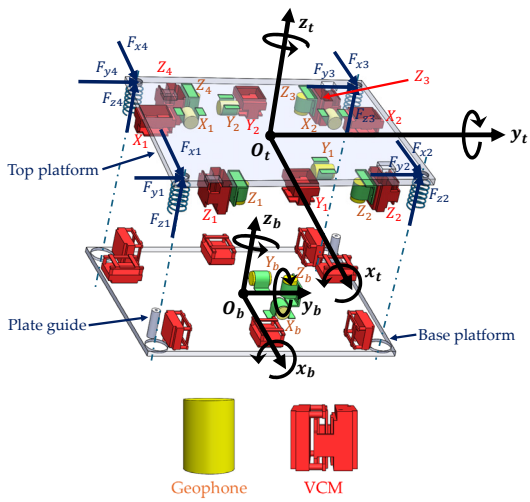

Fig. 1 Schematic drawing of the 6-DoF AVIS

two platforms contains four vertical coil springs, serving to support the mass of the top platform. Eight voice coil motors (VCMs), responsible for controlling movement in 6-DoF, are arranged as illustrated in Fig. 1. Each VCM consists of two yokes moving linearly with each other. One yokes attaches to the lower face of the top platform, while the other attaches to the upper face of the base platform. Plate guides are implemented to restrict the movement of the top platform, ensuring the protection of VCMs.

The top platform's coordinate is defined as a right-handed system, in which the z_t-axis is pointing upward, the x_t-axis is pointing forward and the counterclockwise is the positive rotation direction. The origin of the top platform, denoted as O_t, is located at the center of mass of the top platform. The bottom platform's coordinate system is defined in a similar manner.

The four vertical VCMs (Z_1, Z_2, Z_3, Z_4) produce linear forces in the z_t-direction. Additionally, the two horizontal VCMs (X_1, X_2) generate forces in the x_t-direction, while the other two horizontal VCMs (Y_1, Y_2) produce forces in the y_t-direction. The AVIS motion is monitored by 11 geophone sensors. On the top platform, eight geophone sensors correspond to eight VCMs. In the base platform, three sensors collect velocity in the x_b, y_b and z_b directions, respectively.

The control force of the actuators is denoted $\boldsymbol{U_a} = [F_{vx1}\ F_{vx2}\ F_{vy1}\ F_{vy2}\ F_{vz1}\ F_{vz2}\ F_{vz3}\ F_{vz4}]^T$, where

- F_{vx1}, F_{vx2}: linear forces in the x_t-direction;
- F_{vy1}, F_{vy2}: linear forces in the y_t-direction;
- $F_{vz1}, F_{vz2}, F_{vz3}, F_{vz4}$: linear forces in the z_t-direction.

The dimension of the AVIS is defined as below:

- l_{vjni}; $j,\ n = x,\ y,\ z;\ i = 1,...,4$: distance from the actuator j_i to the center of mass of the top platform in the n_t-direction;
- l_{ni}; $n = x,\ y;\ i = 1,...,4$: distance from the spring i to the center of mass of the top platform in the n_t-direction;
- l_z: distance along the z_t-direction from the center of mass of the top platform to the bottom face of the top platform;
- *l, w, h:* length, width, and height of the top platform respectively.

2.2 System Dynamics

To design a proper controller for a 6-DoF AVIS, the dynamics of the system must be analyzed. The system dynamics can be expressed by the following equation:[1-2,9)]

$$\boldsymbol{M_T}\ddot{\boldsymbol{x}}_t + \boldsymbol{A_2}\dot{\boldsymbol{x}}_t + \boldsymbol{A_1}\boldsymbol{x}_t = \boldsymbol{D_2}\dot{\boldsymbol{x}}_b + \boldsymbol{D_1}\boldsymbol{x}_b + \boldsymbol{U_v} \tag{1}$$

where:

- $\boldsymbol{x_t} = [x_t\ \ y_t\ \ z_t\ \ \theta_{xt}\ \ \theta_{yt}\ \ \theta_{zt}]^T$: the motion vector of the top platform, $\theta_{xt}, \theta_{yt}, \theta_{zt}$: rotations about x_t-, y_t-, and z_t-axes of the top platform.
- $\boldsymbol{x_b} = [x_b\ \ y_b\ \ z_b\ \ \theta_{xb}\ \ \theta_{yb}\ \ \theta_{zb}]^T$: the ground vibration vector, $\theta_{xb}, \theta_{yb}, \theta_{zb}$: rotations about the x_b -, y_b-, and z_b-axes of the bottom platform.
- $\boldsymbol{U_v} = [F_{vx}\ \ F_{vy}\ \ F_{vz}\ \ M_{\theta x}\ \ M_{\theta y}\ \ M_{\theta z}]^T$: the control vector in 6-DoF. F_{vj} is the total control force in the corresponding j_t-direction, $M_{\theta j}$ is the total control torque in the j_t-direction.

The coefficient matrices of equation (1) are given by:

$$\boldsymbol{M_T} = diag\{m, m, m, J_x, J_y, J_z\}, \tag{2}$$

$$\boldsymbol{A_1} = \begin{bmatrix} -4k_x & 0 & 0 \\ 0 & -4k_y & 0 \\ 0 & 0 & -4k_z \\ 0 & 4l_z k_y & 0 \\ -4l_z k_x & 0 & k_z a_1 \\ 0 & -k_y a_1 & 0 \end{bmatrix} \cdots$$

$$\begin{bmatrix} 0 & -4l_z k_x & 0 \\ 4l_z k_y & 0 & -k_y a_1 \\ 0 & k_z a_1 & 0 \\ -k_z a_2 - 4k_y l_z^2 & 0 & 0 \\ 0 & -k_z a_3 - 4k_x l_z^2 & 0 \\ 0 & 0 & -k_x a_2 - k_y a_3 \end{bmatrix},$$

$$\boldsymbol{A_2} = \begin{bmatrix} -4c_x & 0 & 0 \\ 0 & -4c_y & 0 \\ 0 & 0 & -4c_z \\ 0 & 4l_z c_y & 0 \\ -4l_z c_x & 0 & c_z a_1 \\ 0 & -c_y a_1 & 0 \end{bmatrix} \cdots$$

$$\begin{bmatrix} 0 & -4l_z c_x & 0 \\ 4l_z c_y & 0 & -c_y a_1 \\ 0 & c_z a_1 & 0 \\ -c_z a_2 - 4c_y l_z^2 & 0 & 0 \\ 0 & -c_z a_3 - 4c_x l_z^2 & 0 \\ 0 & 0 & -c_x a_2 - c_y a_3 \end{bmatrix},$$

$$\boldsymbol{D_1} = \begin{bmatrix} 4k_x & 0 & 0 \\ 0 & 4k_y & 0 \\ 0 & 0 & 4k_z \\ 0 & -4l_z k_y & 0 \\ 4l_z k_x & 0 & -k_z a_1 \\ 0 & k_y a_1 & 0 \end{bmatrix} \cdots$$

$$\begin{bmatrix} 0 & 4l_z k_x & 0 \\ -4l_z k_y & 0 & k_y a_1 \\ 0 & -k_z a_1 & 0 \\ k_z a_2 + 4k_y l_z^2 & 0 & 0 \\ 0 & k_z a_3 + 4k_x l_z^2 & 0 \\ 0 & 0 & k_x a_2 + k_y a_3 \end{bmatrix},$$

$$\boldsymbol{D_2} = \begin{bmatrix} 4c_x & 0 & 0 \\ 0 & 4c_y & 0 \\ 0 & 0 & 4c_z \\ 0 & -4l_z c_y & 0 \\ 4l_z c_x & 0 & -c_z a_1 \\ 0 & c_y a_1 & 0 \end{bmatrix} \cdots$$

$$\begin{bmatrix} 0 & 4l_z c_x & 0 \\ -4l_z c_y & 0 & c_y a_1 \\ 0 & -c_z a_1 & 0 \\ c_z a_2 + 4c_y l_z^2 & 0 & 0 \\ 0 & c_z a_3 + 4c_x l_z^2 & 0 \\ 0 & 0 & c_x a_2 + c_y a_3 \end{bmatrix}$$

in which:

- $\begin{cases} a_1 = (l_{x1} + l_{x2} - l_{x3} - l_{x4}) \\ a_2 = (l_{y1}^2 + l_{y2}^2 + l_{y3}^2 + l_{y4}^2) \\ a_3 = (l_{x1}^2 + l_{x2}^2 + l_{x3}^2 + l_{x4}^2) \end{cases}$,
- m: the sprung mass;
- k_j, c_j; $j = x, y, z$: stiffness and damping ratio of the spring along the j_t-direction assume that the springs act as linear springs;
- J_j; $j = x, y, z$: the inertia tensor element of the sprung mass in the corresponding j_t-direction with the assumption that the inertia tensor matrix is diagonal.

2.3 System Transfer Matrix

The system dynamics can be transformed into the state-space form as equation (3):

$$\begin{aligned} \dot{\boldsymbol{X}} &= \boldsymbol{AX} + \boldsymbol{BU}_v + \boldsymbol{DX}_b, \\ \boldsymbol{Y} &= \boldsymbol{CX} \end{aligned} \tag{3}$$

in which

- $\boldsymbol{X} = \left[\boldsymbol{x_t}^T \ \dot{\boldsymbol{x}}_t^T\right]^T$: the state vector;
- $\boldsymbol{Y} = \dot{\boldsymbol{x}}_t$: the system output vector;
- $\boldsymbol{X_b} = \left[\boldsymbol{x_b}^T \ \dot{\boldsymbol{x}}_b^T\right]^T$: the vector of vibrations from the bottom platform.

The coefficient matrices of (3) are given by:

$$\begin{aligned} \boldsymbol{A} &= \begin{bmatrix} \boldsymbol{0}_{6\times6} & \boldsymbol{I}_{6\times6} \\ \boldsymbol{M}_T^{-1}\boldsymbol{A}_1 & \boldsymbol{M}_T^{-1}\boldsymbol{A}_2 \end{bmatrix}, \\ \boldsymbol{B} &= \left[\boldsymbol{0}_{6\times6} \ \boldsymbol{I}_{6\times6}\right]^T, \ \boldsymbol{C} = \left[\boldsymbol{0}_{6\times6} \ \boldsymbol{I}_{6\times6}\right], \\ \boldsymbol{D} &= \begin{bmatrix} \boldsymbol{0}_{6\times6} & \boldsymbol{0}_{6\times6} \\ \boldsymbol{M}_T^{-1}\boldsymbol{D}_1 & \boldsymbol{M}_T^{-1}\boldsymbol{D}_2 \end{bmatrix} \end{aligned} \tag{4}$$

where $\boldsymbol{0}_{6\times6}$ denotes the 6-by-6 zero matrix, $\boldsymbol{I}_{6\times6}$ denotes the 6-by-6 identity matrix.

By applying equation (5), the transfer function matrix of the system (3) is obtained in the following form of equation (6):[10]

$$\boldsymbol{G}(s)=\frac{\boldsymbol{Y}(s)}{\boldsymbol{U_v}(s)}=\boldsymbol{C}(s\boldsymbol{I}-\boldsymbol{A})^{-1}\boldsymbol{B} \tag{5}$$

$$\boldsymbol{G}(s)=\begin{bmatrix} G_{11}(s) & 0 & G_{13}(s) & 0 & G_{15}(s) & 0 \\ 0 & G_{22}(s) & 0 & G_{24}(s) & 0 & G_{26}(s) \\ G_{31}(s) & 0 & G_{33}(s) & 0 & G_{35}(s) & 0 \\ 0 & G_{42}(s) & 0 & G_{44}(s) & 0 & G_{46}(s) \\ G_{51}(s) & 0 & G_{53}(s) & 0 & G_{55}(s) & 0 \\ 0 & G_{62}(s) & 0 & G_{64}(s) & 0 & G_{66}(s) \end{bmatrix} \tag{6}$$

In equation (6), $G_{ii}(s)$, $i=1,...,6$, are the transfer functions in the diagonal line of $\boldsymbol{G}(s)$. That is, $G_{ii}(s)$ is the ratio between the Laplace transform of the velocity in the i^{th} direction and the Laplace transform of the applying force/torque in this direction. $G_{in}(s)$, $n=1,...,6$, $i\neq n$, are the remaining other transfer functions. In other words, $G_{in}(s)$ are the transfer functions of the interferences. These interferences act as internal disturbances, affecting the performance of the system.

3. Robust Decoupling Controller Design

The main objective of the controller for the AVIS is to isolate the external vibration, hence the top platform is stabilized. Additionally, equation (6) shows that there are interferences in the system. To successfully eliminate the mutual interferences, the feedforward compensators is added. Finally, a feedback controller is designed based on the H_∞ control framework to ensure the system's stability and robustness.

3.1 Feedforward Control Law

To begin with, from equation (6), the system can be rewritten as follows:

$$\begin{aligned} \boldsymbol{Y}(\boldsymbol{s}) &= \boldsymbol{G}(s)\,\boldsymbol{U_v}(s) \\ &= \left[G_{ii}(s)\right]\boldsymbol{H}(s)\,\boldsymbol{U_v}(s), \\ \boldsymbol{H}(s) &= \boldsymbol{I_{6\times 6}}+\left[G_{ii}(s)\right]^{-1}\left[G_{in}(s)\right] \end{aligned} \tag{7}$$

in which $\left[G_{ii}(s)\right]$ is the diagonal matrix from the diagonal line of $\boldsymbol{G}(s)$ and $\left[G_{in}(s)\right]$ is the matrix containing the remainder. It is noted that (7) only exists if the transfer function $G_{ii}(s)^{-1}G_{in}(s)$ is proper and analytic functions for every i and n.[10] Additionally, by defining $\boldsymbol{U_k}(s)=\boldsymbol{H}(s)\,\boldsymbol{U_v}(s)$, equation (7) becomes:

$$\boldsymbol{Y}(s)=\left[G_{ii}(s)\right]\boldsymbol{U_k}(s) \tag{8}$$

$\boldsymbol{U_k}(s)$ acts as the control input for the system of the diagonal elements $\left[G_{ii}(s)\right]$, i.e, the system without interferences. Then, once the control input $\boldsymbol{U_k}(s)$ is obtained, and if $\boldsymbol{H}(s)$ is invertible, $\boldsymbol{U_v}(s)$ can be obtained by:

$$\boldsymbol{U_v}(s)=\boldsymbol{H}(s)^{-1}\boldsymbol{U_k}(s) \tag{9}$$

Besides, from equation (7), $\boldsymbol{U_v}(s)$ can be equivalently written as follows:

$$\begin{aligned} &\boldsymbol{U_v}(s)=\boldsymbol{U_k}(s)-\boldsymbol{U_f}(s), \\ &\boldsymbol{U_f}(s)=\left[G_{ii}(s)\right]^{-1}\left[G_{in}(s)\right]\boldsymbol{U_v}(s) \\ &=\begin{bmatrix} G_{11}^{-1}(s)\,G_{13}(s)F_z(s)+G_{11}^{-1}(s)\,G_{15}(s)M_{\theta y}(s) \\ G_{22}^{-1}(s)\,G_{24}(s)M_{\theta x}(s)+G_{22}^{-1}(s)\,G_{26}(s)M_{\theta z}(s) \\ G_{33}^{-1}(s)\,G_{31}(s)F_x(s)+G_{33}^{-1}(s)\,G_{35}(s)M_{\theta y}(s) \\ G_{44}^{-1}(s)\,G_{42}(s)F_y(s)+G_{44}^{-1}(s)\,G_{46}(s)M_{\theta z}(s) \\ G_{55}^{-1}(s)\,G_{51}(s)F_x(s)+G_{55}^{-1}(s)\,G_{53}(s)F_z(s) \\ G_{66}^{-1}(s)\,G_{62}(s)F_y(s)+G_{66}^{-1}(s)\,G_{64}(s)M_{\theta x}(s) \end{bmatrix} \end{aligned} \tag{10}$$

in which $\boldsymbol{U_f}(s)$ is the feedforward element.

In equation (10), one can see that for each DoF of the AVIS, the total control input consists of the corresponding control for the system without interference and the feedforward control from the inputs of the interacting directions. Therefore, the feedforward eliminates the mutual interferences among the movements.

3.2 Feedback Control Law

In this study, the mixed sensitivity H_∞ control is applied for designing $\boldsymbol{U_k}(s)$, thanks to its effectiveness and efficiency in handling complex systems with uncertainties.[11-13] Fig. 2 illustrates the configuration of the control for the entire 6-DoF AVIS. Fig. 3 demonstrates how the controller works for each DoF of the system. In which, $\boldsymbol{K}(s)$ is the feedback control transfer matrix, and $\boldsymbol{W_1}(s)$, $\boldsymbol{W_2}(s)$, $\boldsymbol{W_3}(s)$ are the proper and analytic frequency-dependent weighting functions. It is noted that the mutual interferences between each channel are eliminated by the use of feedforward. Nevertheless, these compensators themselves are considered disturbances to the system. Hence, the weighting function $\boldsymbol{W_1}(s)$ is chosen corresponding to the control effort without the feedforward compensator. $\boldsymbol{W_2}(s)$ is to suppress the total disturbances. $\boldsymbol{W_3}(s)$ corresponds to the system outputs. The functions are selected based on the system characteristics and designer experience, ensuring each exceeds the corresponding maximum singular values in the system. Then, the closed-loop transfer function can be expressed as:[11-14]

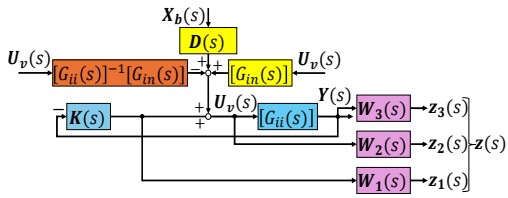

Fig. 2 Schematic drawing of the proposed control for 6-DoF AVIS

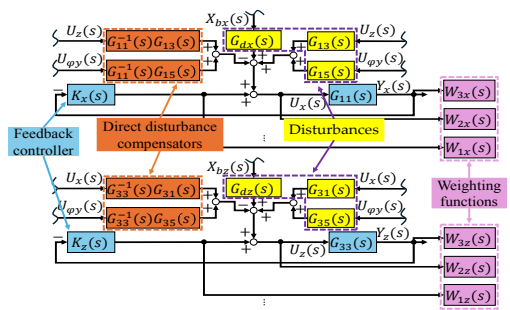

Fig. 3 Schematic drawing of the proposed control for the x_t- and z_t-directions of the AVIS

$$\boldsymbol{M}(s)=\begin{bmatrix}-\boldsymbol{W_1}(s)\boldsymbol{K}(s)\boldsymbol{T}(s)\\ \boldsymbol{W_2}(s)\boldsymbol{S}(s)\\ \boldsymbol{W_3}(s)\boldsymbol{T}(s)\end{bmatrix} \tag{11}$$

where:

- $\boldsymbol{S}(s)=\left(\boldsymbol{I_{6\times6}}+\left[G_{ii}(s)\right]\boldsymbol{K}(s)\right)^{-1}$;
- $\boldsymbol{T}(s)=\left[G_{ii}(s)\right]\left(\boldsymbol{I_{6\times6}}+\left[G_{ii}(s)\right]\boldsymbol{K}(s)\right)^{-1}$;
- $\boldsymbol{W_i}(s)$, $i=1,2,3$, are diagonal:

$$\begin{aligned}\boldsymbol{W_i}(s)=diag\{&W_{ix}(s),W_{iy}(s),W_{iz}(s),\\&W_{i\theta x}(s),W_{i\theta y}(s),W_{i\theta z}(s)\}\end{aligned} \tag{12}$$

The mixed sensitivity problem can be described as finding $\boldsymbol{K}(s)$ to stabilize the closed-loop system and minimizing the H_∞ norm of $\boldsymbol{M}(s)$.[11-14] The resulting controller matrix $\boldsymbol{K}(s)$ is in the following form:

$$\begin{aligned}\boldsymbol{K}(s)=diag\{&K_x(s),\ K_y(s),\ K_z(s),\\&K_{\theta x}(s),\ K_{\theta y}(s),\ K_{\theta z}(s)\}\end{aligned} \tag{13}$$

in which $K_j(s)$ is the controller corresponding to the j_t-direction, $j=x,\ y,\ z,\ \theta_x,\ \theta_y,\ \theta_z$. The complete control law of the AVIS is written by:

$$\boldsymbol{U_v}(s)=\boldsymbol{K}(s)\boldsymbol{Y}(s)-\left[G_{ii}(s)\right]^{-1}\left[G_{in}(s)\right]\boldsymbol{U_v}(s) \tag{14}$$

Then, the control forces $\boldsymbol{U_a}$ of the eight actuators can be simply obtained as follows:

$$\boldsymbol{U_a}=\boldsymbol{B_a^+}\boldsymbol{U_v},$$
$$\boldsymbol{B_a^+}=\boldsymbol{B_a^T}(\boldsymbol{B_a}\boldsymbol{B_a^T})^{-1},$$
$$\boldsymbol{B_a}=\begin{bmatrix}1&1&0&0&0&0&0&0\\0&0&1&1&0&0&0&0\\0&0&0&0&1&1&1&1\\0&0&l_{vyz}&l_{vyz}&-l_{vzy1}&l_{vzy2}&l_{vzy3}&-l_{vzy4}\\-l_{vxz}&-l_{vxz}&0&0&-l_{vzx1}&-l_{vzx2}&l_{vzx3}&l_{vzx4}\\l_{vxy1}&-l_{vxy2}&l_{vyx1}&-l_{vyx2}&0&0&0&0\end{bmatrix} \tag{15}$$

4. Simulation Results and Discussion

4.1 System Implementation

The algorithm implementation of the proposed controller is described in the following steps: (1) The system parameters are determined; (2) The feedforward control is constructed as in equation (10); (3) The H_∞-based controller is computed by using the function 'mixsyn' in Mathworks MATLAB; and (4) The order of the controller is reduced using the balanced truncation method with the focus frequency range is from 0.01 to 100 [Hz]. Additionally, a PID controller are designed for the AVIS for comparison:

$$U_v = K_P x_t + K_I \int_0^t x_t dt + K_D \dot{x}_t \quad (20)$$

Table 1 Platforms specifications

Parameter	Value
$l,\ w,\ h$ [mm]	465, 366, 12
$l_{x1}, l_{x2}, l_{x3}, l_{x4}$ [mm]	161.3, 161.3, 170.7, 170.7
$l_{y1}, l_{y2}, l_{y3}, l_{y4}$ [mm]	215.5, 215.5, 215.5, 215.5
l_z [mm]	1.5
k_x, k_y, k_z [N/m]	12683, 12683, 22526.2
c_x, c_y, c_z [Ns/m]	9.087, 9.087, 26.64
m [kg]	9.085
J_x, J_y, J_z [kg.m^2]	0.1218, 0.1656, 0.2838

in which K_P, K_I, K_D are diagonal matrices of parameters of the PID controller for each DoF. The

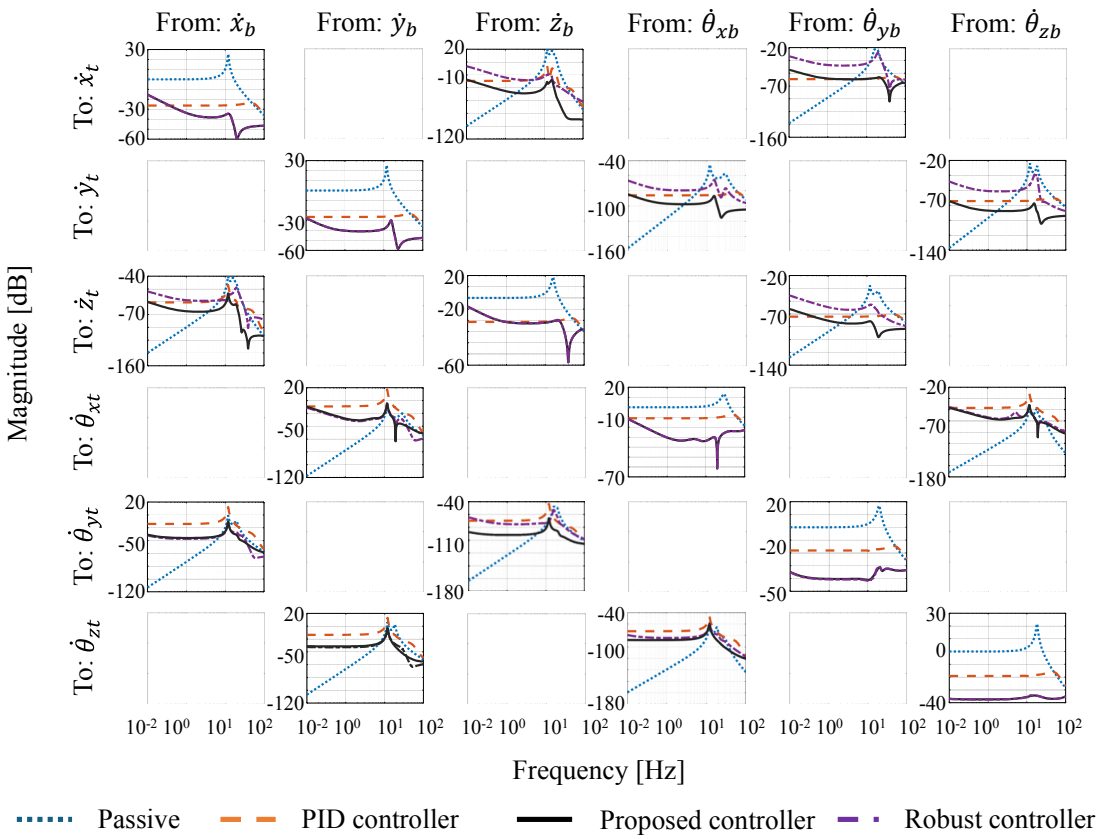

Fig. 4 Frequency responses of top platform

Table 2 PID controllers' parameters

Controller	Parameters		
	K_P	K_I	K_D
PID_x	2454.24	1002258.19	50.50
PID_y	2414.58	1017554.05	70
PID_z	2241.54	966652.73	90
$PID_{\theta x}$	27.19	10943.67	1.2
$PID_{\theta y}$	41.74	17293.58	1.5
$PID_{\theta z}$	72.91	29759.60	2.5

parameters of the PID controller are selected by trial-and-error method with the assistance of the PID Tuner app in Mathworks MATLAB. The response time is 0.002s, the rise time is at most 0.00218, the settling time is at most 0.0164s, and the overshoot is at most 10.5%. The parameters of the 6-DoF AVIS and the PID controllers are respectively listed in Tables 1 and 2. Additionally, the weighting function matrices $\boldsymbol{W_i}(s)$ are listed in Appendix.

4.2 Simulation Results

The simulation is carried out using MATLAB/Simulink. The performance is tested by the chirp signal, which denotes the vibration from the ground. The chirp signal has amplitude of 0.001 [m/s] and a frequency range span from 0.01 to 100 [Hz]. Moreover, the controller also needs to handle mutual interferences from other directions.

Fig. 4 shows the vibration isolation results in all directions using an array of the frequency responses – the Bode plots. The row represents ground vibration ($\dot{\boldsymbol{x}}_{\boldsymbol{b}}$), while the column represents the motion of the top platform ($\dot{\boldsymbol{x}}_{\boldsymbol{t}}$). Each plot in the diagonal line is the frequency response of the system in one direction corresponding to the ground vibration in the same direction. The remainders in the figure represent the effect of the disturbances other directions. For instance, for a ground vibration in the x_b-direction, the responses

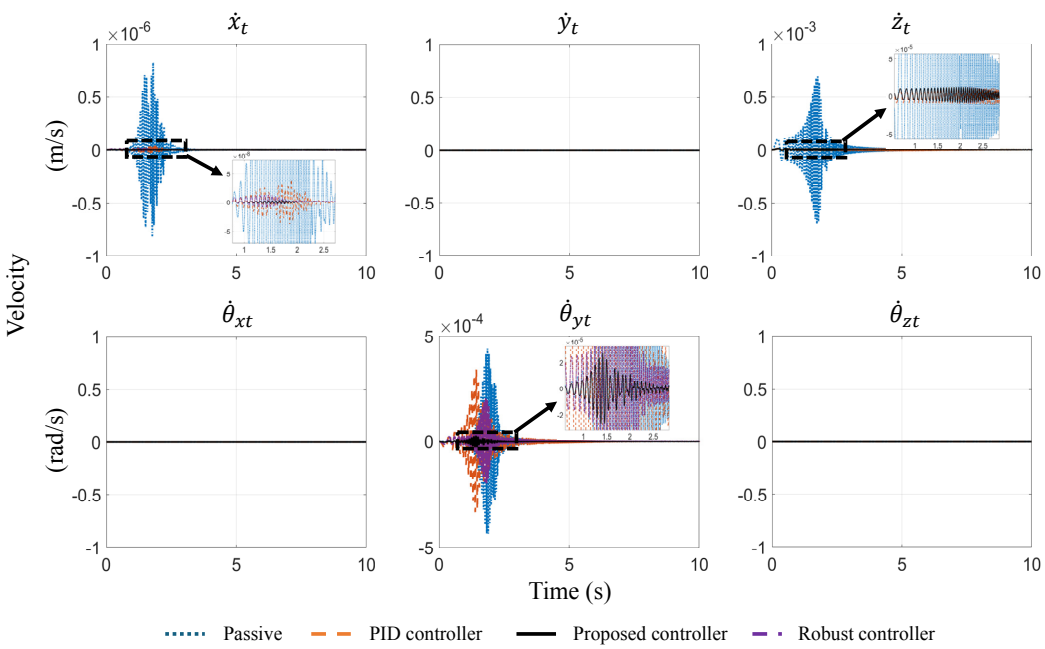

Fig. 5 The velocities at the center of the top platform in case of disturbance in z_b-direction

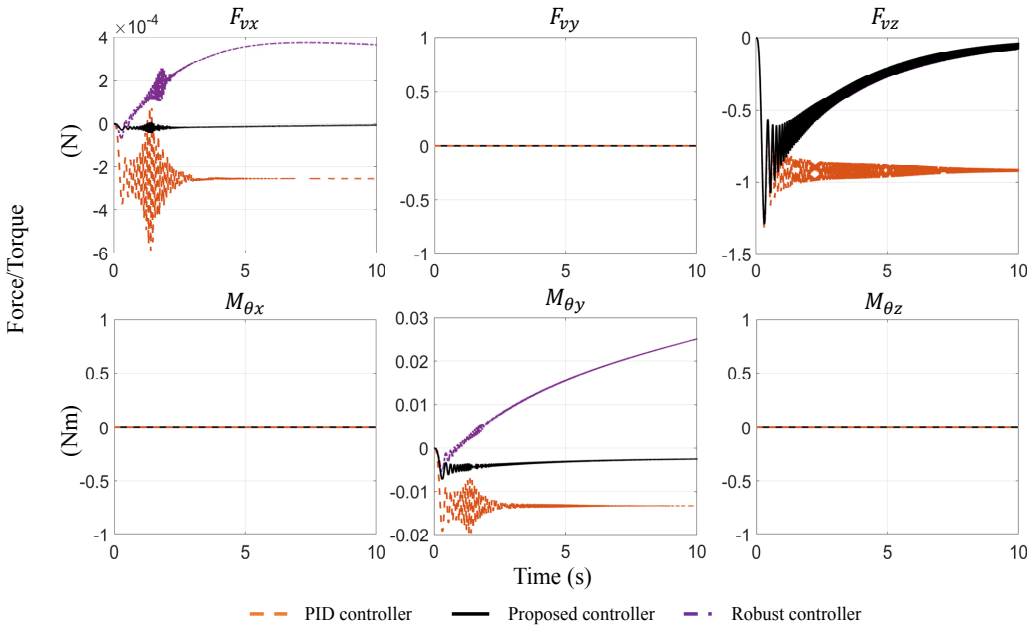

Fig. 6 The control effort of the controllers – robust decoupling controller, robust controller, and PID controller - in case of disturbance in z_b-direction.

of the top platform are shown in the first column in the figure. The first graph is the frequency response also in the x_t-direction. The other two graphs are the motion in the z_t and θ_{yt}-direction.

The passive system, the spring-mass-damper system, can suppress the vibration in the high-frequency but suffers from an unwanted phenomenon, the resonant peak in the diagonal element. This resonant peak occurs at a frequency of around 20 [Hz], amplifies rather than suppresses vibrations. The robust decoupling controller provides a good vibration isolation performance over all frequencies. For the interferences, the proposed controller has an effect in a range of frequencies, around 15 to 80 [Hz]. The robust controller without feedforward and PID controller also proves to be efficiency in the main direction, as evident from the six graphs along the diagonal line in the Fig. 4. In these instances, it effectively suppress the vibration and stabilizes the top platform against the disturbance from the ground. However, when it comes to the interference suppression, the robust controller and PID controller proves ineffective. This is particularly noticeable in the non-diagonal graphs of the Fig. 4. In comparison with the proposed controller, the PID controllers is not effective enough in most of the frequencies, even in the main direction, where the PID controller achieves the most vibration isolation performance. In the interference suppression, the PID controller almost has no effect, making it less effective than the proposed controller, which works well across a wider range of frequencies. On the other hand, the robust controller without the feedforward maintains almost identical performance in the main direction in comparison with the robust decoupling controller, however, the results of the interference direction are not effective as the proposed controller especially in the translational motions.

To further clarify the vibration isolation performance, the vibration isolation results in case of ground vibration in the z_b-direction only is presented in Fig. 5. In the translational direction x_t and z_t, the PID controller has an impressive effect on stabilizing the top platform, indicating in the velocities $\dot{x}_t$ and $\dot{z}_t$ in the first and third graphs. However, the PID controller is not as effective as the robust decoupling controller. In the rotational direction $\dot{\theta}_{yt}$, the PID controller performance is far from the performance of the robust decoupling controller. The velocities in case of PID controller are the least impressive, following by the robust controller without feedforward and the best results are the robust decoupling controller. The velocities in the remaining graphs $\dot{y}_t$, $\dot{\theta}_{xt}$ and $\dot{\theta}_{zt}$ are very small. Fig. 6 represents the control effort of the PID controller, the robust controller and the robust decoupling controller. During the initial one second, the control efforts of the three controllers are closely align. However, beyond this point, the proposed controller seems to be more responsive to the disturbance than the remaining controllers. Consequently, the PID controller proves to be less effective. The control efforts of the robust decoupling controller are smallest compares with the PID controller and the robust controller. The control efforts in the remaining graphs F_{vy}, $M_{\theta x}$ and $M_{\theta z}$ are very small (approximately 10^{-16}).

5. Conclusions

This paper describes basic background, a brief development of an active vibration isolation system and presents the robust decoupling control system design for 6-Dof AVIS. The velocity sensors are used to collect the motion of the system, the robust decoupling controller is successfully designed to control the motion of the 6-DoF AVIS via the VCMs. The simulation result shows that the proposed robust decoupling controller proves to be efficiency to isolate the external disturbances, suppress the mutual interferences and hence, stabilize the system. The effect of feedforward control is also presented. In comparison with the PID controller, the robust decoupling controller proves to be more efficiency, especially in suppressing the mutual interferences. In the future, the experiment will be conducted to verify the efficiency of the proposed controller.

Acknowledgement

This work was supported by the National Research Foundation (NRF), South Korea under Project BK21 FOUR (Smart Convergence and Application Education Research Center). This work was also supported by the National Research Foundation of Korea (NRF) grant funded by the Korean government (MSIT) (No. 2022R1A2C1003486).

Author contributions

Y. B. Kim; Conceptualization, Supervision and Project administration. D. H. Lee; Investigation and methodology. T. N. Nguyen; Software, formal analysis, data curation, visualization, writing-original draft. T. Huynh; Conceptualization, methodology, validation, writing-review & editing. T. N. Nguyen and T. Huynh contributed equally to this work.

Appendix

The weighting functions are listed as follows:

$$W_{1x}(s) = \frac{0.3237s^2 + 1200s + 1.292e05}{s^2 + 4.69s + 5807},$$

$$W_{2x}(s)=\frac{0.001091s^5+0.3644s^4+291.3s^3...}{s^5+568.5s^4+61210s+1.041e07s^2...}\\ \frac{+5708s^2+60400s+72740}{+1.084e08s+1.672e08},$$

$$W_{3x}(s)=\frac{0.06983s^2+4.316s+110}{s^2+14.42s+4868},$$

$$W_{1y}(s)=\frac{0.9184s^2+5525s+6.029e05}{s^2+1.287s+6242},$$

$$W_{2y}(s)=\frac{0.006723s^5+2.164s^4+592.3s^3...}{s^5+295.1s^4+24400s^3...}\\ \frac{+2.994e04s^2+3.216e04s+2.985e04}{+4.354e06s^{2+}2.097e06s+4.405e06},$$

$$W_{3y}(s)=\frac{0.05549s^2+6.971s+182.9}{s^2+0.4902s+5234},$$

$$W_{1z}(s)=\frac{0.204s^2+1169s+8.779e05}{s^2+8.798s+10510},$$

$$W_{2z}(s)=\frac{0.005075s^4+1.408s^3+645.3s^2...}{s^4+329.4s^3+31110s^2...}\\ \frac{+14800s+6584}{+4.031e06s+1.596e06},$$

$$W_{3z}(s)=\frac{0.0005342s^2+15.23s+491.8}{s^2+74.4s+24700},$$

$$W_{1\varphi x}(s)=\frac{0.072s^2+4179s+6.737e06}{s^2+12.05s+13810},$$

$$W_{2\varphi x}(s)=\frac{0.1s^5+106.2s^4+9914s^3...}{s^5+245.8s^4+16140s^3...}\\ \frac{+1.531e06s^2+7.478e07s+5.052e09}{+3.514e06s^2+6.385e07s+1.209e10},$$

$$W_{3\varphi x}(s)=\frac{0.053s^2+228.9s+647.2}{s^2+47.18s+34260},$$

$$W_{1\varphi y}(s)=\frac{0.2s^2+1.127e04s+1.782e07}{s^2+12.5s+14110},$$

$$W_{2\varphi y}(s)=\frac{0.22s^5+335.1s^4+3.134e04s^3...}{s^5+244.5s^4+16150s^3...}\\ \frac{+4.463e06s^2+2.136e08s+1.552e10}{+3.502e06s^2+6.284e07s+1.21e10},$$

$$W_{3\varphi y}(s)=\frac{0.005s^2+3.498s+9.204}{s^2+11.84s+14440},$$

$$W_{1\varphi z}(s)=\frac{0.052s^2+3037s+4.912e06}{s^2+12.33s+13890},$$

$$W_{2\varphi z}(s)=\frac{0.1s^5+109.2s^4+1.019e04s^3...}{s^5+246.8s^4+16120s^3...}\\ \frac{+1.569e06s^2+7.658e07s+5.172e09}{+3.512e06s^2+6.384e07s+1.208e10},$$

$$W_{3\varphi z}(s)=\frac{0.005s^2+3.73s+9.514}{s^2+10.94s+14430}$$

References

1. D. J. Inman, 2017, Vibration with Control, 2nd Edition, John Wiley & Sons, Hoboken, New Jersey, 4-21. (DOI:10.1002/0470010533)
2. A. Preumont, 2018, “Vibration Control of Active Structures: An Introduction”, Springer Dordrencht, Dordrencht Netherlands, 1-44. (DOI:10.1007/978-94-007-2033-6)
3. C. C. Fuller, S. Elliott and P. A. Nelson, 1996, “Active Control of Vibration, Academic Press, Massachusetts”, USA, 185-221. (DOI:10.1016/B978-0-12-269440-0.X5000-6)
4. G. Genta, 2009, “Vibration Dynamics and Control”, Springer, New York, USA, 135-211. (DOI:10.1007/978-0-387-79580-5)
5. M. R. Hatch, 2000, “Vibration Simulation Using MATLAB and ANSYS”, CRC press, Florida, USA, 1-50. (DOI:10.1201/9781420035759)
6. D. H. Lee et al., 2021, “Noninteracting Control Design for 6-DoF Active Vibration Isolation Table with LMI Approach”, Applied Sciences. 11(16), 7693. (DOI:10.3390/app11167693)
7. D. Jiang et al., 2020, “Modeling identification and control of a 6-DOF active vibration isolation system driving by voice coil motors with a Halbach array magnet”, Journal of Mechanical Science and Technology, 34, 617-630. (DOI:10.1007/s12206-019-1208-y)
8. M. H. Kim et al., 2016, “Design and Control

of a 6-DOF Active Vibration Isolation System Using a Halbach Magnet Array", IEEE/ASME Transactions on Mechatronics, 21(4), 2185-2196. (DOI:10.1109/TMECH.2016.2539349)

9. S. S. Rao, 2010, "Mechanical Vibrations, 5th Edition", Prentice Hall, New York, USA, 769-869.
10. C. T. Chen, 2014, "Linear System Theory and Design: International Fourth Edition", Oxford University Press, Oxford, England, 6-55.
11. U. Mackenroth, 2004, "Robust Control Systems: Theory and Case Studies", Springer, 201-485.
12. K. Zhou and J. C. Doyle, 1998, "Essentials of Robust Control", Prentice Hall, New Jersey, USA, 269-348. (DOI:10.1201/b11313)
13. D. W. Gu, P. Petkov and M. M. Konstantinov, 2013, "Robust Control Design with MATLAB®, 2nd Edition", Springer London, London, England, 31-64. (DOI:10.1007/978-1-4471-4682-7)
14. L. Fortuna, M. Frasca and A. Buscarino, 2022, "Optimal and Robust Control: Advanced Topics with MATLAB®, 2nd Edition", CRC press, Florida, USA, 195-208. (DOI:10.1201/9781003196921)